Evolutions of Micro- and Macrostructure by Cerium Treatment in As-Cast AISI M42 High-Speed Steel

WEI-CHAO JIAO, HUA-BING LI, HAO FENG, ZHOU-HUA JIANG, LING-FENG XIA, SHU-CAI ZHANG, HONG-CHUN ZHU, and WEI WU

The as-cast M42 high-speed steels containing different contents of cerium (Ce) were manufactured to investigate the effects of Ce on the solidification structures at the micro- and macroscale. The results indicate that the addition of Ce could modify $MgO{\cdot}Al_2O_3$ and MnS into the Ce-containing inclusions. The addition of Ce refined the dendrite structure and eutectic carbides, which can be ascribed to the heterogeneous nucleation of primary austenite on Ce_2O_2S or Ce_2O_3 and the increase in both the compositional supercooling at the dendrite forefront and the restriction on the dendrites coarsening. Both the secondary dendrite arm spacing (SADS) and total eutectic carbides content decrease gradually with increasing Ce content. M_2C and M_6C carbides are the predominant precipitates. The increase of Ce content made the morphology of M_2C carbides change from long lamellar or straight-rod morphology into shorter curved-rod or honeycomb morphology because of the overgrowth of eutectic austenite, but it had no significant effect on the morphology of M_6C carbides. Ce_2O_2S and Ce_2O_3 can serve as the very effective heterogeneous nucleation sites for M_6C carbides because of the low lattice disregistry between them, hence Ce addition improved markedly the macroscopic distribution of M_6C carbides in the cast ingot and promoted the formation of M_6C carbides at the expense of M_2C carbides.

https://doi.org/10.1007/s11663-020-01912-x

I. INTRODUCTION

AISI M42, a molybdenum-series high-speed steel (HSS) with an additional 8 wt pct cobalt, has been extensively employed in cutting tools manufacturing owing to its harmonious combination of high hardness, superior hot hardness, excellent wear resistance and good toughness.[1,2] Traditionally, M42 HSS is produced in the route as follows: ingot casting → hot forging and hot rolling → heat treatment.[3,4] However, due to the low cooling rate and the severe segregation of alloying elements (C, Mo, Cr, W, V, *etc.*) during solidification, the as-cast structure of M42 HSS inevitably contains comparably high proportion of coarse eutectic carbides (including MC, M_2C and M_6C) heterogeneously distributed along the interdendritic regions.[1–6] These coarse eutectic carbides significantly decrease the hot workability of steel, thus leading to increased forging scrap rate.[3,7] Meanwhile, they are apt to form large-size and uneven carbide bands even after a substantial amount of hot plastic deformation, deteriorating the toughness and isotropic properties of steel.[2,8–11] In addition, the difference in the cooling rate from the center to the edge of the cast ingot results in a serious non-uniform distribution of M_6C eutectic carbides at the macroscopic scale.[1,12] Therefore, improving the as-cast structure is of significance for M42 HSS to obtain the superior overall performance.

In order to solve above-mentioned problems, an idea option is to use the rapid solidification technologies like powder metallurgy and spray forming, which can enormously eliminate the segregation of alloying elements and achieve fine and uniformly distributed eutectic carbides.[13–15] However, complicated process and high costs restrict their wide application and large-scale industrial production.[7,16,17] Under such condition, ingot casting modification by adding some amounts of modifying agents (different chemical elements) into the molten steel becomes the first selected option. Several recent studies have shown that adding rare earth metals like cerium (Ce) and lanthanum (La)

WEI-CHAO JIAO, HAO FENG, LING-FENG XIA, SHU-CAI ZHANG, and HONG-CHUN ZHU are with the School of Metallurgy, Northeastern University, No. 3-11, Wenhua Road, Heping District, Shenyang 110819, P.R. China. HUA-BING LI and ZHOU-HUA JIANG are with the School of Metallurgy, Northeastern University and also with the State Key Laboratory of Rolling and Automation, Northeastern University, No. 3-11, Wenhua Road, Heping District, Shenyang, 110819, P.R. China. Contact e-mail: lihb@smm.neu.edu.cn WEI WU is with the Metallurgical Technology Institute, Central Iron & Steel Research Institute, No. 76, Xueyuan Nanlu, Haidian District, Beijing, 100081, P.R. China.

Manuscript submitted February 27, 2020.
Article published online July 24, 2020.

can produce some beneficial effects on the microstructures and properties of HSS. Li *et al.*[18] and Zhou *et al.*[19] reported that introducing Ce to M2 HSS can refine the dendritic structure and the plate-like M_2C eutectic carbide and alleviate the segregation of alloying elements (Mo, W, V, Cr, *etc.*). Liu *et al.*[20] found that adding mischmetal (Ce-La) to M2 HSS can promote the separation and spheroidization of eutectic carbides during subsequent heat treatment, and thereby enhance the impact toughness and bending strength of the steel. Fu *et al.*[21] and Yang *et al.*[22] demonstrated that adding Ce to high carbon HSS (Fe-5Mo-5Cr-5V-5W-3Nb-2C) can induce change in the morphology of eutectic carbides from network-like structure to granulation (particularly after heat treatment), thus enhancing the impact toughness and facture toughness of the steel. Therefore, adding rare earth metals is a promising method for improving the as-cast structure and service properties of M42 HSS, while the correlative researches are still almost blank. Moreover, previous researches have rarely focused on the effects of rare earth metals on the inclusions and macrostructure of HSS.

Therefore, in this work, four M42 HSS cast ingots containing different Ce contents (0, 0.03, 0.16 and 0.27 wt pct, respectively) were manufactured. The aim is to investigate the effects of Ce on the inclusion behavior, dendrite structure and eutectic carbides characteristics (amount, size, type, morphology and distribution) of the as-cast M42 HSS.

II. EXPERIMENTAL

A. *Materials Preparation*

In the present study, four M42 HSS cast ingots containing different Ce contents (given as Ce0, Ce0.03, Ce0.16 and Ce0.27, respectively) were prepared using a 25 kg pressurized induction furnace,[23] and their alloy compositions were summarized in Table I. The quantity of raw materials added to the steel was given in Table II, and the smelting process was summarized in steps as follows:

(i) Pure Fe (99.90 pct), Co (99.98 pct), Mo (99.98 pct), W (99.95 pct), Cr (99.32 pct) and Si (99.37 pct) were put into a crucible made of $MgO{\cdot}Al_2O_3$ and melted at 1873 K (1600 °C) under Ar atmosphere.
(ii) Pure C (99.95 pct) was added into the molten steel. About 3 minutes later, vacuum pumps were activated to decrease the gas pressure in the furnace to 5 Pa (about 20 minutes), which is known as vacuum carbon-deoxidization. Afterwards, high-purity Ar (99.999 pct) was piped into the furnace until the gas pressure in the furnace increased to 20000 Pa.
(iii) Afterwards, pure Al (99.99 pct) was added into the molten steel for further deoxydization.
(iv) About 3 minutes later, pure Mn (99.80 pct) and V (99.95 pct) were added into the molten steel.
(v) About 3 minutes later, pure Ce (99.5 pct) was added into the molten steel.
(vi) About 3 minutes later, the molten steel was poured into a cast iron mold at approximately 1823 K (1550 °C).

B. *Analysis Method*

For the chemical analysis, the total oxygen (T.O) content of the steel was determined using LECO TC500 Oxygen-Nitrogen analyzer. The contents of carbon and sulfur were analyzed with ELTRA CS-3000 Carbon-Sulfur analyzer. The contents of aluminum, magnesium and cerium were analyzed with VARIAN 725-ES inductively coupled plasma atomic emission spectroscopy (ICP-AES). The contents of other elements were analyzed with ARL-4460 direct reading spectrometer.

The cast ingot is in the shape of a 260-mm-high truncated cone, with a bottom diameter of 95 mm and a top diameter of 110 mm. All the test specimens used in this paper were cut from the same positions of each ingot, as illustrated in Figure 1. The as-cast microstructures and inclusions were analyzed *via* OLYMPUS DSX510 optical microscopy (OM) and ZEISS ULTRA PLUS scanning electron microscopes (SEM) with an energy dispersive spectrometry (EDS). The specimens were firstly prepared by standard grinding and polishing procedures.[24] For the inclusion analysis, the polished specimens were used. For the as-cast microstructure analysis, the polished specimens for OM observations were etched using Groesbeck reagent (H_2O:K_2MnO_4:NaOH = 23:1:1 (in weight percent)), and the polished specimens for SEM observations were etched with Nital reagent (C_2H_5OH:HNO_3 = 9:1 (in volume percent)). The number and size of inclusions (at least 400 particles per specimen) were analyzed using Image-pro Plus 6.0 software on SEM images.[25] The analyzing area of Ce0, Ce0.03, Ce0.16 and Ce0.27 steels are about 1.04, 0.62, 0.42 and 0.42 mm^2, respectively. The SDAS and the area fraction of eutectic carbides were estimated using OLYCIA m3 metallographic image analysis software.[26]

In order to investigate the types of carbides in the steel, the electrolytic extraction method was used.[27,28] The cuboid specimens with a size of 50 mm × 10 mm × 10 mm were adopted as the cathode and were electrolyzed in organic solution (CH_3OH:HCl:ZnCl:citric acid = 90.4:5:3.6:1 (in weight percent)). The total current and temperature were controlled to be less than 1.0 A and 5 °C, respectively. Afterwards, the collected carbides powder was examined by RIGAKU SMARTLAB X-ray diffraction (XRD) in a range of 30 to 100 deg and at a scan rate of 2 deg/min. In order to reveal the macroscopic distribution of eutectic carbides, a disc was cut out from the cast ingot at a height ranging from 140 to 150 mm and ground with the grinding machine, and finally etched with Nital reagent.

III. RESULTS

A. *Inclusion Analysis*

Figure 2 shows the SEM images and EDS analyses of typical inclusions in the M42 cast ingots with different Ce contents. In the absence of Ce, the inclusions in the steel can be divided into two categories: (i) single inclusions including spherical $MgO{\cdot}Al_2O_3$ (Figure 2(a)) and irregular blocky MnS (Figure 2(b)); (ii) composite

Table I. Alloy Compositions of the M42 HSS Cast Ingots (Weight Percent)

No.	C	Mo	Co	Cr	W	V	Si	Mn	Al	Mg	T.O	S	Ce	Fe
Ce0	1.14	9.46	7.97	3.73	1.49	1.13	0.28	0.26	0.017	0.0007	0.0014	0.0036	—	bal.
Ce0.03	1.13	9.48	7.96	3.72	1.47	1.14	0.29	0.28	0.019	0.0011	0.0013	0.0025	0.03	bal.
Ce0.16	1.14	9.48	7.98	3.74	1.49	1.13	0.27	0.28	0.022	0.0014	0.0010	0.0024	0.16	bal.
Ce0.27	1.14	9.47	7.98	3.71	1.48	1.12	0.28	0.27	0.037	0.0021	0.0010	0.0023	0.27	bal.

Table II. The Quantity of Raw Materials Added to the Steel (g)

No.	C	Mo	Co	Cr	W	V	Si	Mn	Al	Fe	Ce
Ce0	241.4	1996.0	1680.3	793.3	315.2	241.8	62.1	67.9	2.04	15624.5	0
Ce0.03	241.5	1996.2	1680.0	773.1	315.5	242.1	62.1	68.1	2.06	15614.9	20.7
Ce0.16	241.4	1996.8	1680.4	793.3	315.2	241.8	62.1	67.8	2.06	15614.8	52.7
Ce0.27	241.4	1996.0	1680.0	792.8	315.5	242.2	62.1	67.9	2.05	15605.6	104.0

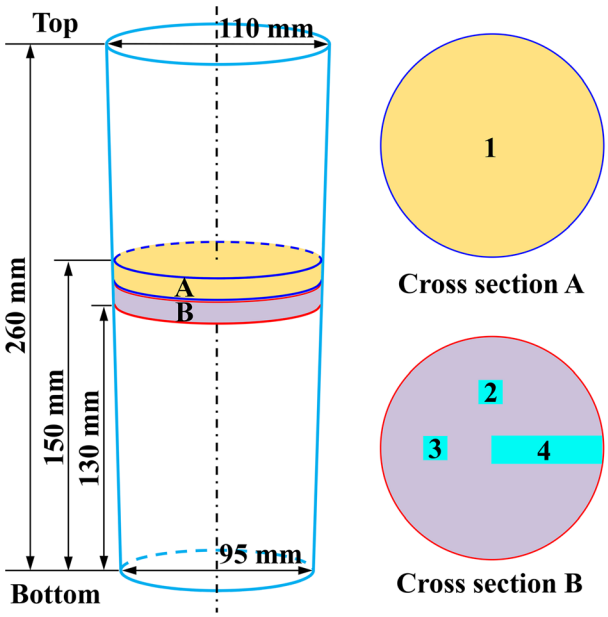

1 : Macroscopic observation of eutectic carbides distribution;

2 and **3** : Metallographic samples for analysis, 8 × 8 × 10 mm;

4 : Electrolytic extraction of precipitates, 10 × 10 × 50 mm;

Fig. 1—Schematic diagram of the cast ingot and the sampling positions.

inclusions of $MgO{\cdot}Al_2O_3$ wrapped by MnS (Figure 2(c)). After adding 0.03 wt pct Ce into the steel, only spherical or ellipsoidal cerium oxy-sulfides were detected and generally considered as Ce_2O_2S,[29,30] as illustrated in Figures 2(d) through (f). When the Ce contents are 0.16 and 0.27 wt pct, besides cerium oxy-sulfides (Figures 2(g), (h), (j) and (k)), irregular blocky cerium oxides were also detected and generally considered as Ce_2O_3 (Figures 2(i) and (l)).[31,32] Moreover, it can be observed that cerium oxides have a larger size than cerium oxy-sulfides.

Figure 3 shows the inclusion size distribution of M42 cast ingots with different Ce contents and the variation of the number density (N_A) and average size (d) of inclusions with the Ce content. As shown in Figure 3(a), Ce content of 0.03 wt pct has little influence on the inclusion size distribution, and the majority of inclusions in Ce0 and Ce0.03 cast ingots are less than 1.0 μm in size. When the Ce contents are 0.16 and 0.27 wt pct, the proportions of inclusions in the size range of 1 to 2 and 2 to 3 μm increase dramatically, and some large inclusions with a size of more than 3 μm are also formed. From Figure 3(b), it can be observed that both the average inclusion size and the number density of inclusions gradually increase with increasing Ce content. High inclusion number density will increase the probability of collision and aggregation of inclusions.[33] Therefore, in the present study the average inclusion size has the same trend with the inclusion number density.

B. *As-Cast Structure Analysis*

The typical as-cast microstructures of M42 cast ingots with different Ce contents are shown in Figure 4. As can be seen, the main microstructural constituents are dendrites of iron matrix (bright regions) and networks of eutectic carbides (dark-gray regions) distributed along the interdendritic regions. Moreover, it can be clearly observed that the dendrite structure and eutectic carbides of M42 cast ingot are refined by Ce addition. For clarity, the SDAS and the area fraction of eutectic carbides were measured, as shown in Figure 5. Statistical results indicate that as the Ce content increases from 0.00 to 0.27 wt pct, the SDAS decreases from 45.3 to 33.3 μm and the area fraction of eutectic carbides decreases from 19.1 to 14.5 pct.

In order to investigate the microsegregation behavior of alloying elements in the steel, the EDS chemical distribution maps of Ce0.16 steel are given in Figure 6. It is found that Co element segregated into the dendrite region during solidification (Figure 6(b)), indicating that the equilibrium partition coefficient of Co is more than

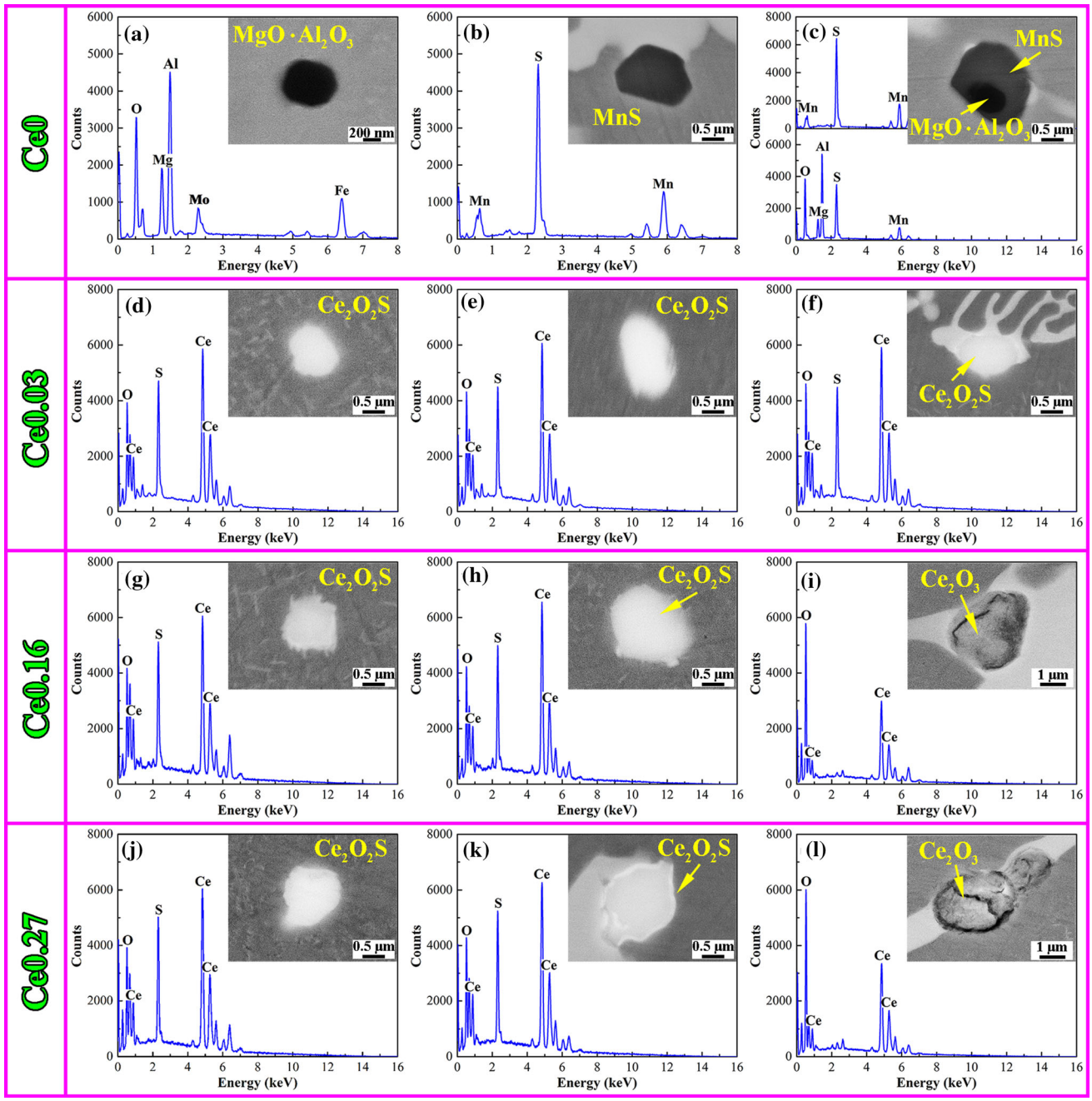

Fig. 2—SEM images and EDS analyses of typical inclusions in the M42 cast ingots with different Ce contents. (*a*) to (*c*) Ce0; (*d*) to (*f*) Ce0.03; (*g*) to (*i*) Ce0.16; (*j*) to (*l*) Ce0.27.

1. Mo, Cr, W, V, C and Ce elements segregated to interdendritic region during solidification and were enriched in eutectic carbides (Figures 6(c) through (h)), which indicates that the equilibrium partition coefficient of these elements are less than 1. In addition, it can be clearly observed that Ce element was also enriched in cerium oxides and cerium oxy-sulfides (Figures 6(h) and (i)).

Figure 7 gives the XRD patterns of the carbides extracted from the M42 cast ingots with different Ce contents. It is found that the carbides in four cast ingots are all composed of hexagonal Mo-rich M_2C carbides, cubic Fe-rich and Mo-rich M_6C carbides as well as cubic V-rich MC carbides. Thus, the addition of Ce has no important influence on the carbide type. Furthermore, the relative intensity of diffraction peaks indicates that M_2C and M_6C carbides are always the predominant precipitates in the cast ingots. Therefore, the effects of Ce on M_2C and M_6C carbides were mainly investigated.

The typical morphology of M_2C and M_6C carbides in the M42 cast ingots with different Ce contents are shown in Figure 8. In the absence of Ce, M_2C carbides mainly exhibit long lamellar or straight-rod morphology (Figure 8(a)). After adding 0.03 wt pct Ce into the steel,

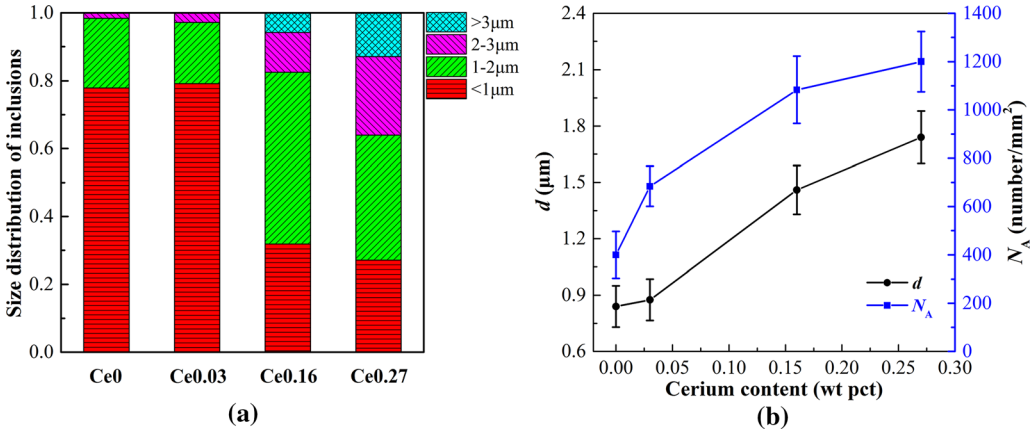

Fig. 3—(*a*) The inclusion size distribution of M42 cast ingots with different Ce contents, (*b*) the variation of the number density N_A and average size *d* of inclusions with the Ce content.

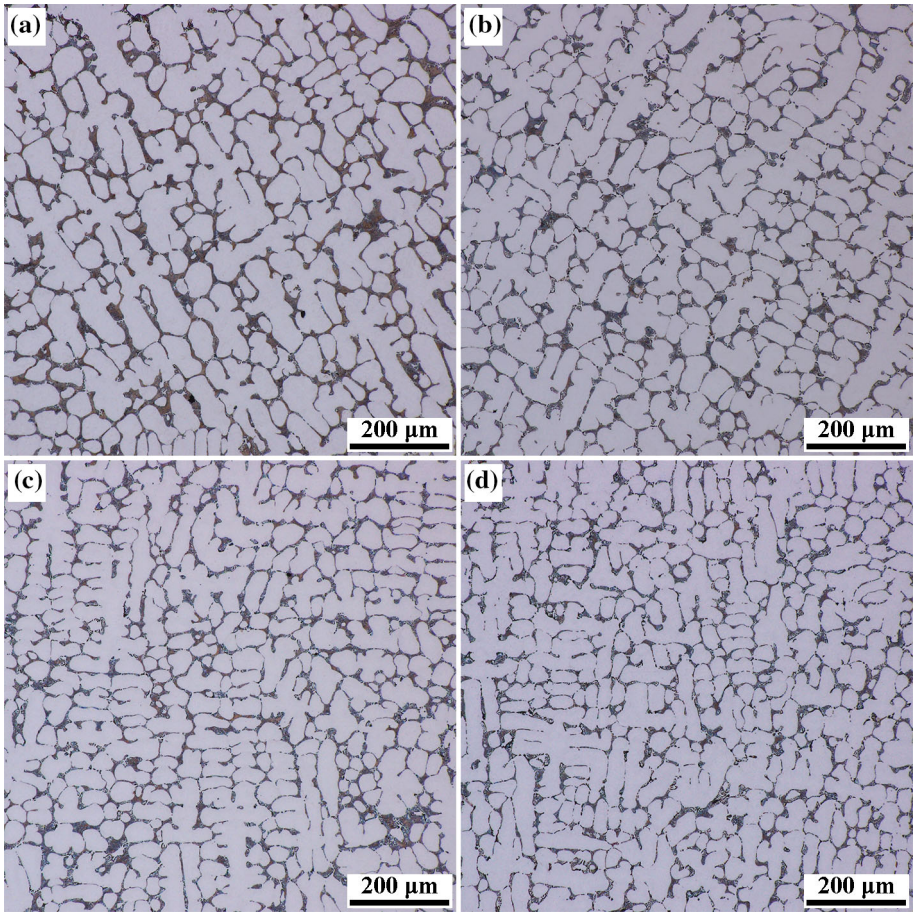

Fig. 4—The typical as-cast microstructures of M42 cast ingots with different Ce contents. (*a*) Ce0; (*b*) Ce0.03; (*c*) Ce0.16; (*d*) Ce0.27.

M_2C carbides mainly present shorter straight-rod or curved-rod morphology (Figure 8(b)). When the Ce contents are 0.16 and 0.27 wt pct, M_2C carbides mainly exhibit curved-rod or honeycomb morphology (Figures 8(c) and (d)). As shown in Figures 8(e) through (h), the morphology of M_6C carbides in four cast ingots is all characterized by the presence of a central platelet, form which arises many secondary platelets separated from each other by the matrix. This morphological characteristic is called fishbone morphology by previous researchers.[1,13] Therefore, the addition of Ce can significantly change the morphology of M_2C carbides, but it has little influence on the morphology of M_6C carbides.

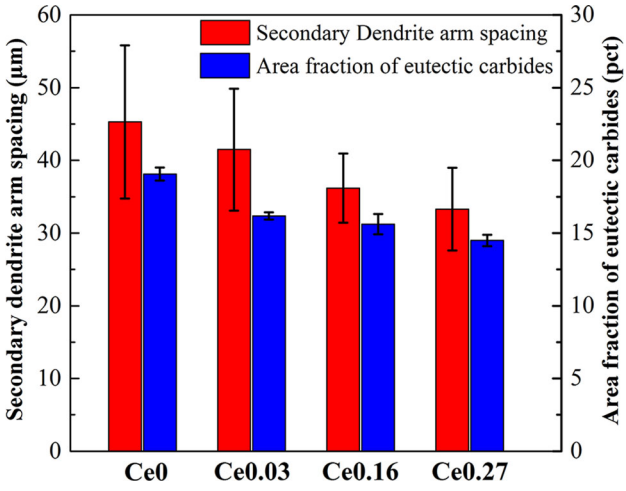

Fig. 5—The SDAS and eutectic carbides area fraction of M42 cast ingots with different Ce contents.

Figure 9 shows the as-cast macrostructure on the cross section of M42 cast ingots with different Ce contents. It can be observed that there exist many bright white regions on the cross section. In order to better understand the macrostructure of M42 cast ingots, the microstructures of different regions in Ce0 steel are shown in Figure 10. It is found that the bright white region is mainly composed of iron matrix and M_6C carbides (Figure 10(c)), and the rest of region is the mixture of iron matrix and M_2C carbides (Figure 10(b)). This result is consistent with our previous reports.[1,12] In this paper, the bright white region is called as the M_6C region. As shown in Figure 9(a), M_6C regions of Ce0 steel are mainly distributed in the center of the cross section and exhibit a large block-like morphology. After adding 0.03 wt pct Ce into the steel, M_6C regions exhibit a small dot-like morphology and were relatively uniformly distributed throughout the cross section, as shown in Figure 9(b). When the Ce contents are 0.16

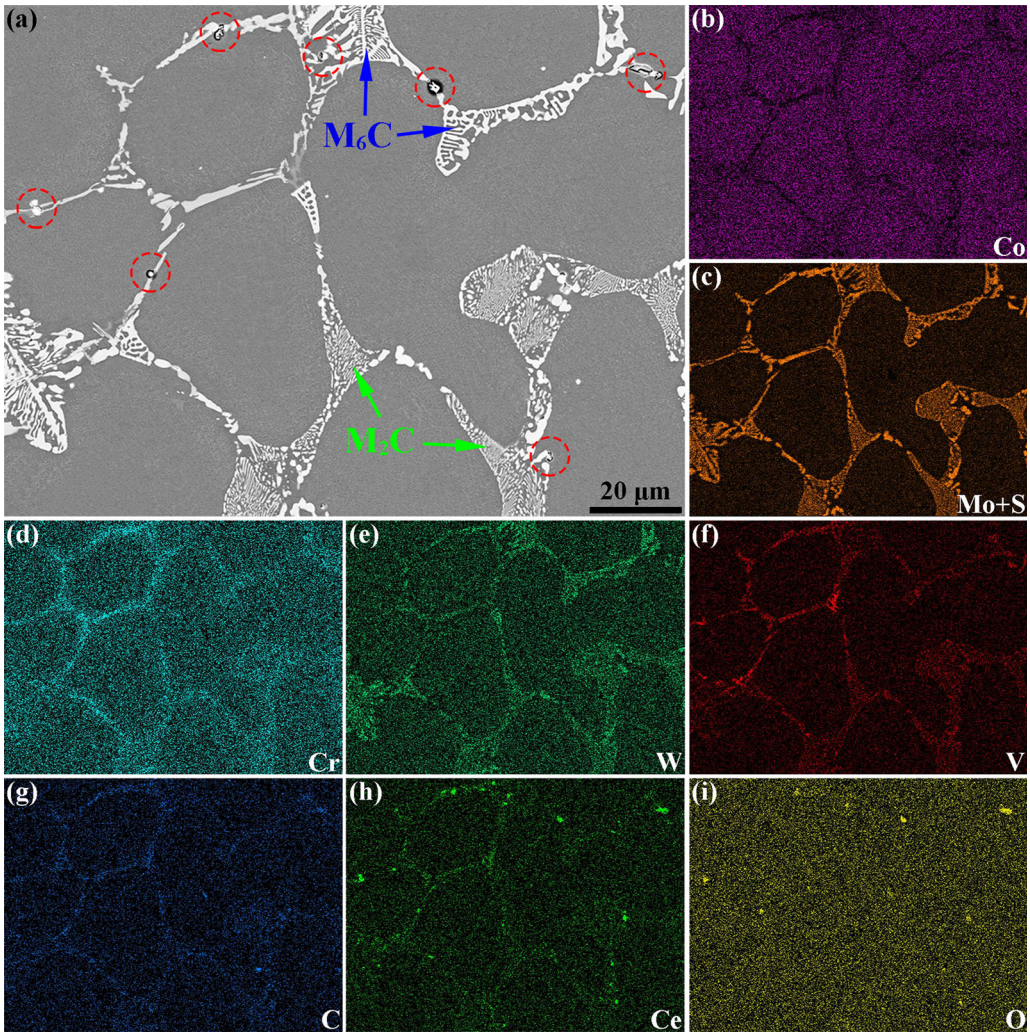

Fig. 6—(*a*) SEM micrograph showing the microstructure of Ce0.16 steel. Related EDS mapping showing the distribution of (*b*) Co, (*c*) Mo/S, (*d*) Cr, (*e*) W, (*f*) V, (*g*) C, (*h*) Ce and (*i*) O.

and 0.27 wt pct, the amount of dot-like M_6C regions is remarkably increased and M_6C regions are uniformly distributed throughout the cross section, as shown in Figures 9(c) and (d). The above results indicate that the addition of Ce can significantly improve the macroscopic distribution of M_6C carbides and favors the formation of M_6C carbides compared to M_2C carbides.

IV. DISCUSSION

A. *Refining Mechanism of Dendrite Structure*

The results as shown in Figures 4 and 5 indicate that the dendrite structure of M42 HSS is gradually refined with the increase of Ce content. The following reasons can account for this result. Previous studies have shown that inclusion induced heterogeneous nucleation often occurs during solidification in Ce-containing steel. As shown in Figures 2 and 6(a), Ce addition can form high melting point of cerium oxy-sulfides (Ce_2O_2S) or cerium oxides (Ce_2O_3). These Ce-containing inclusions can steadily exist in the molten steel as solid particles because the Gibbs free energies of formation of these inclusions are far less than 0 even at high temperature of 1773 K (1500 °C).[34,35] Thus, Ce_2O_2S and Ce_2O_3 are the possible nucleants for primary austenite (γ-Fe). To theoretically estimate the effectiveness of Ce_2O_2S and Ce_2O_3 as heterogeneous nucleation sites for primary austenite, the lattice disregistry between them was calculated using the Bramfitt two-dimensional disregistry model. The formula is expressed as follows[36,37]:

$$f_{(hkl)_n}^{(hkl)_s} = \sum_{i=1}^{3} \frac{\left| d_{[uvw]_s^i} \cos\theta - d_{[uvw]_n^i} \right|}{3 \times d_{[uvw]_n^i}} \times 100\,\text{pct}, \qquad [1]$$

where f is the lattice disregistry; $(hkl)_s$ and $(hkl)_n$ are the low-index face of the substrate and the nucleated phase, respectively; $[uvw]_s$ and $[uvw]_n$ are the low-index direction of $(hkl)_s$ and $(hkl)_n$, respectively; $d_{[uvw]_s}$ and $d_{[uvw]_n}$ are the interatomic spacing along direction $[uvw]_s$ and $[uvw]_n$, respectively; and θ is the angle between $[uvw]_s$ and $[uvw]_n$. The crystallographic information of γ-Fe, Ce_2O_2S and Ce_2O_3 are given in Table III,[31,37–39] and the lattice disregistry between γ-Fe and Ce_2O_2S or Ce_2O_3 are given in Table IV. The lattice disregistry between $(0001)Ce_2O_2S$ and $(100)\gamma$-Fe is about 5.57 pct and that between $(0001)Ce_2O_3$ and $(100)\gamma$-Fe is about 6.33 pct. According to the Bramfitt's criterion,[36,40] the nucleating agent is potent when the lattice disregistry is below 12 pct. Therefore, Ce_2O_2S and Ce_2O_3 can serve as heterogeneous nucleation sites for primary austenite during solidification, which is beneficial to the refinement of the dendrite structure.[12,21]

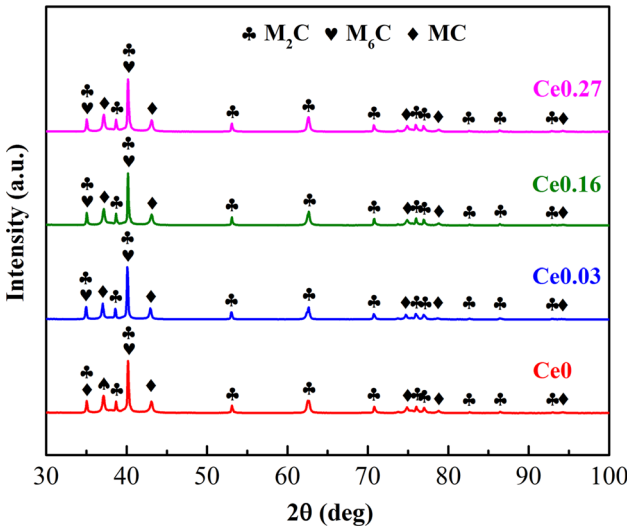

Fig. 7—XRD patterns of the carbides extracted from the M42 cast ingots with the different Ce contents.

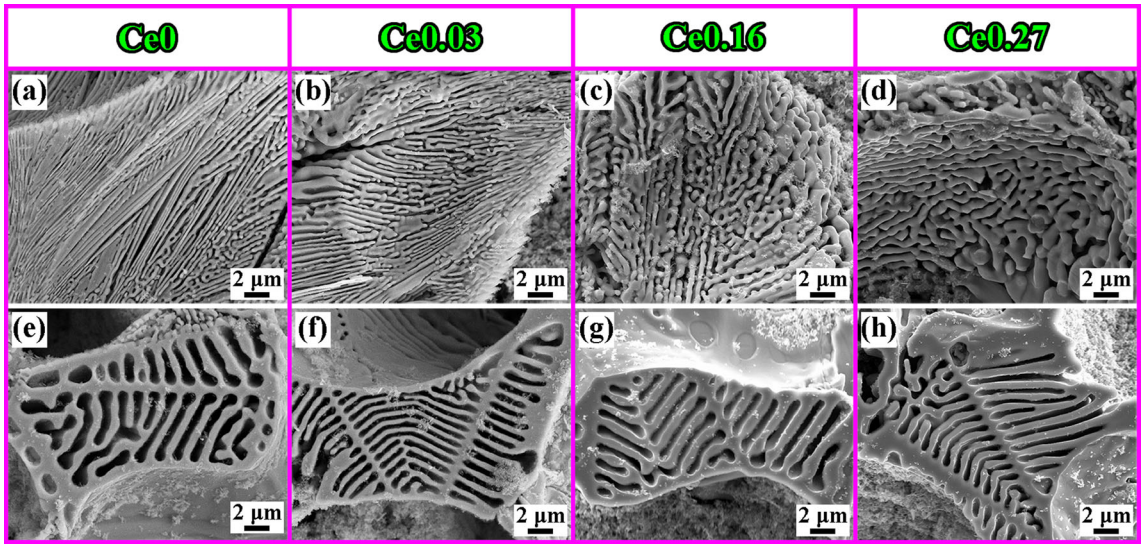

Fig. 8—SEM micrographs showing the morphology of M_2C and M_6C carbides. (*a*) to (*d*) show the morphology of M_2C carbides in Ce0, Ce0.03, Ce0.16 and Ce0.27 steels, respectively. (*e*) to (*h*) show the morphology of M_6C carbides in Ce0, Ce0.03, Ce0.16 and Ce0.27 steels, respectively.

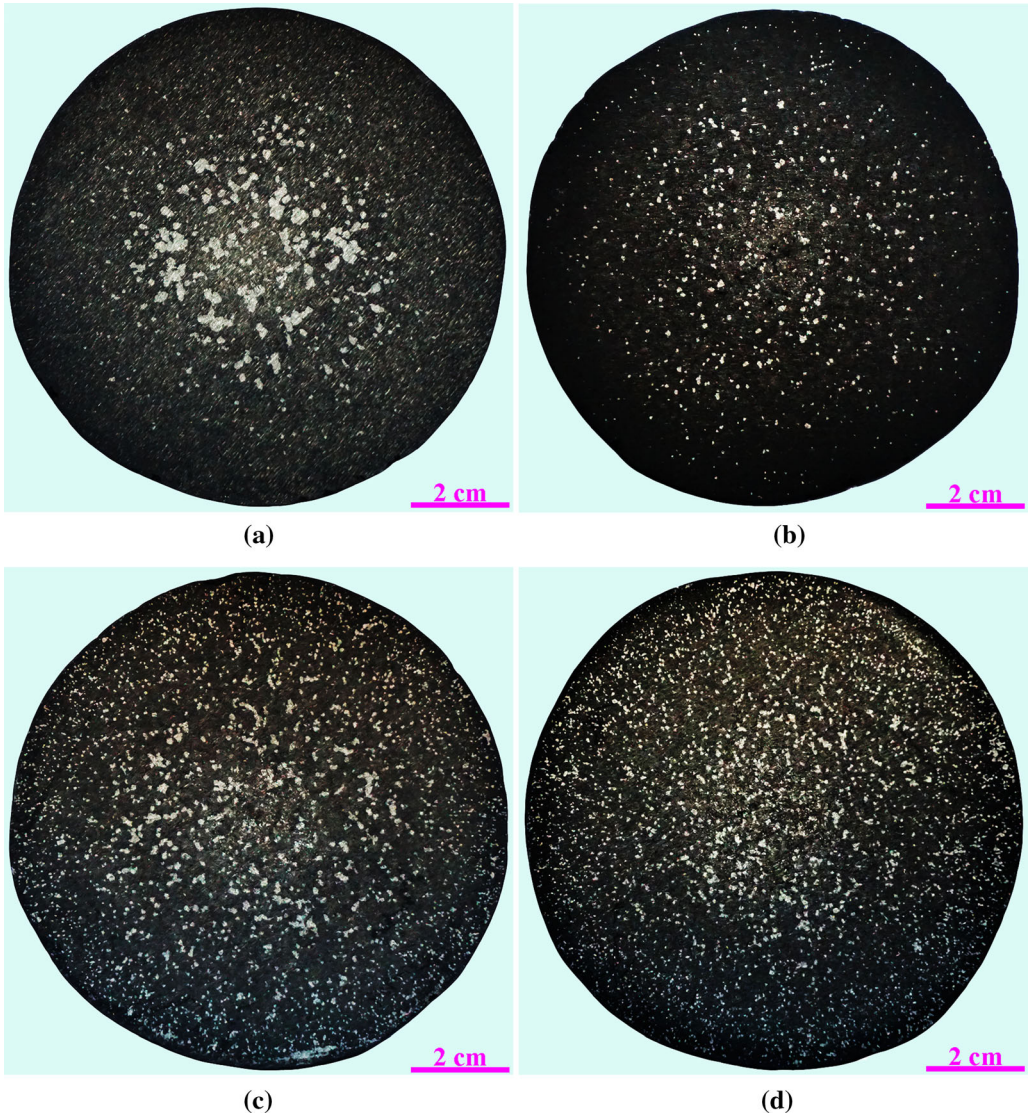

Fig. 9—The as-cast macrostructure on the cross section of M42 cast ingots with different Ce contents. (*a*) Ce0; (*b*) Ce0.03; (*c*) Ce0.16; (*d*) Ce0.27.

In addition to heterogeneous nucleation, the constitutional supercooling and intermetallic phases also have significant effects on the dendrite structure. Due to the low solubility of Ce in austenite phase, the addition of Ce will strongly segregate and enrich into the liquid phase at the dendrite forefront during solidification,[21,41,42] which is confirmed by the experimental result that Ce segregates into the interdendritic regions (Figure 6(h)). Moreover, owing to the strong interaction between Mo/Ce atoms and W/Ce atoms,[43] the enrichment of W and Mo in the liquid phase during solidification would further increase the segregation degree of Ce. The interdendritic segregation of Ce will lead to the increase of constitutional supercooling at the beginning of the solidification, which promotes the branching of dendrites.[21,42] Meanwhile, large-atoms Ce can hinder the growth of dendrites by the drag effect on solid-liquid interface migration.[44] On the other hand, the combined presence of high levels of C, Mo, Cr, W, V and Fe in the interdendritic region produces intermetallic phases (M_2C or M_6C eutectic carbides) at the end of solidification. It has been suggested that the intermetallic phases forming at the end of solidification can effectively prevent the coalescence and coarsening of dendrites.[45–47] The discussion in Section IV–B shows that Ce-containing inclusions can act as the nucleation sites for heterogeneous nucleation of eutectic carbides, which could lead to an increase in the nucleation of eutectic carbides, thus increasing the restriction on the dendrites coarsening.

B. *Evolution Mechanism of Eutectic Carbides*

1. *Size and content of eutectic carbides*

As shown in Figure 4, eutectic carbides of M42 HSS are refined by Ce addition. It has been demonstrated that eutectic carbides in the as-cast HSS are formed by a eutectic reaction (Liquid → austenite + carbides) at the end of solidification, *i.e.*, the residual liquid is decomposed into the eutectic austenite and eutectic carbides

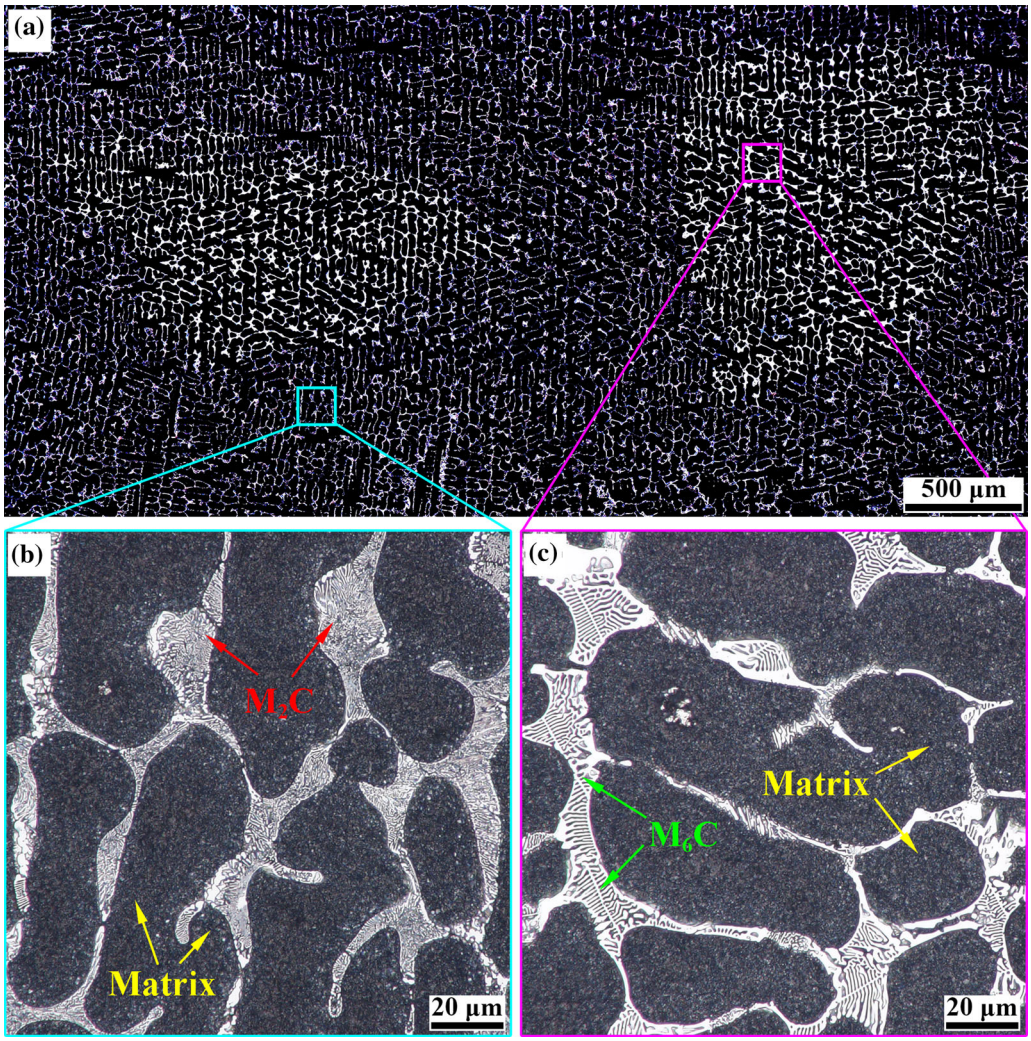

Fig. 10—(*a*) OM micrograph showing the microstructure of Ce0 steel, (*b*) and (*c*) enlarged view of different regions in micrograph (a).

Table III. Crystallographic Information of Phases

Phase	Lattice Structure	Space Group	Lattice Parameter (nm) at 1773 K (1500 °C)	Refs.
γ-Fe	FCC	$Fm\bar{3}m$	$a = 0.369$	31
Ce_2O_2S	HCP	$P\bar{3}m1$	$a = 0.405$	37,38
Ce_2O_3	HCP	$P\bar{3}m1$	$a = 0.394$	39

Table IV. Lattice Disregistry Between γ-Fe and Ce_2O_2S or Ce_2O_3

	Matching Directions		Interatomic Spacing (nm)			
Matching Planes	$[uvw]_s$	$[uvw]_n$	$d[uvw]_s$	$d[uvw]_n$	θ (deg)	f (pct)
$(0001)Ce_2O_2S//(100)\gamma$-Fe	$[\bar{1}2\bar{1}0]$	[010]	0.405	0.369	0	5.57
	$[\bar{2}110]$	[012]	0.810	0.825	3.43	
	$[\bar{1}010]$	[002]	0.702	0.738	0	
$(0001)Ce_2O_3//(100)\gamma$-Fe	$[\bar{1}2\bar{1}0]$	[010]	0.394	0.369	0	
	$[\bar{2}110]$	[012]	0.788	0.825	3.43	6.33
	$[\bar{1}010]$	[002]	0.682	0.738	0	

through the redistribution of alloying elements.[13,48,49] As mentioned above, the addition of Ce can increase the nucleation of primary austenite and promote the branching of dendrites. As a result, eutectic carbides has less space to grow and thus are refined.[50,51] On the other hand, Ce-containing inclusions can act as the heterogeneous nucleation sites for eutectic carbide (see Section IV–B–3), which also favors the refinement of eutectic carbide. In addition, previous researches have shown that the addition of Ce can reduce the activity of C in the molten steel ($e_C^{Ce} < 0$),[18,41] which will cause the eutectic reaction to happen at a relatively higher solid fraction. Therefore, the total eutectic carbides content of the as-cast M42 HSS gradually decreases with the increase of Ce content (Figure 5).

2. *Morphology of eutectic carbides*

The results as shown in Figure 8 indicate that the morphology of M_2C carbides in the as-cast M42 HSS has a significant change by Ce addition. During solidification, M_2C carbides are formed by the eutectic reaction: Liquid $\rightarrow$ austenite + M_2C, in which M_2C carbides preferentially nucleate from the residual liquid and grow as the leading phase.[1,49] As discussed in Section IV–A, Ce has a low solubility in austenite phase. Thus, it will strongly segregate to the solid-liquid interface during the eutectic reaction process, resulting in a high compositional supercooling. This will increase the growth rates of both eutectic austenite and M_2C carbides.[1,52] As a non-faceted phase, the increment in the growth rate of eutectic austenite is more notable than that of M_2C carbides (faceted phase). In order to avoid the overgrowth of eutectic austenite and keep M_2C carbides as the leading phase in the eutectic reaction, M_2C carbides have to bend and branch extensively.[13,52] Therefore, the morphology of M_2C carbides in the as-cast M42 HSS changes from long lamellar or straight-rod morphology into shorter curved-rod or honeycomb morphology with the increase of Ce content. In the present study, the addition of Ce has no significant influence on the morphology of M_6C carbides, which is consistent with the conclusion of Boccalini *et al.* that the morphology of M_6C carbides is not affected by cooling rate or chemical composition.[13]

3. *Macroscopic distribution and content of M_6C carbides*

In addition to the above changes in the microstructures, the addition of Ce also has a significant effect on the macrostructure of the as-cast M42 HSS (Figure 9). It is well known that there exists a competitive nucleation relationship between M_2C and M_6C carbides during solidification, which is closely correlated to their nucleation driving force.[1,13,53] Previous studies have shown that high cooling rate can more remarkably reduce the Gibbs free energy for nucleation of M_2C carbides, thus favoring the formation of M_2C carbides.[1,13] Therefore, compared with the edge of the cast ingot, the center of the cast ingot is more favorable to the precipitation of M_6C carbides because of its lower cooling rate. This reasonably explains why M_6C carbides are mainly distributed in the center of the cast ingot in the absence of Ce (Figure 9(a)). After adding Ce into the steel, M_6C carbides are uniformly distributed in the cast ingots (Figures 9(b) through (d)), and the amount of M_6C carbides shows an increasing tendency with increasing Ce content. The increase of M_6C carbides means the reduction of M_2C carbides. Thus, the addition of Ce favors the formation of M_6C carbides at the expense of M_2C carbides. As shown in Figure 6(a), Ce-containing inclusions (marked with red circles) are frequently observed on eutectic carbides. For the Ce0.03, Ce0.16 and Ce0.27 steels, the amount ratio of the Ce-containing inclusions which are at eutectic carbides to the total Ce-containing inclusions are approximately 14.3, 44.5 and 55.3 pct, respectively. Thus, the above changes in the macrostructure of the as-cast M42 HSS may owe to the nucleation effect of Ce-containing inclusions. Consequently, the lattice disregistry between eutectic carbides (M_2C and M_6C) and Ce-containing inclusions (Ce_2O_2S and Ce_2O_3) were calculated. Based on our previous study,[12] the structure of M_2C carbide is close-packed hexagonal (HCP) with the lattice parameter $a = 0.302$ nm and $c = 0.472$ nm, the structure of M_6C carbide is face-centered cubic (FCC) with the lattice parameter $a = 1.116$ nm. As shown in Table V, the lattice disregistry between (0001)Ce_2O_2S and (0001)M_2C, and (0001)Ce_2O_3 and (0001)M_2C are about 13.81 pct and 11.31 pct, respectively. The lattice disregistry between (0001)Ce_2O_2S and (111)M_6C, and (0001)Ce_2O_3 and (111)M_6C are about 2.65 pct and 0.13 pct, respectively. It is found that M_6C carbides have a much lower lattice disregistry with Ce_2O_2S and Ce_2O_3 than M_2C carbides. This means that Ce_2O_2S and Ce_2O_3 can act as very effective nucleants for M_6C carbides during solidification, thus improving the macroscopic distribution of M_6C carbides in the as-cast M42 HSS and promoting the formation of M_6C carbides. The increase of Ce content leads to a higher number density of Ce_2O_2S and Ce_2O_3, hence more M_6C carbides are formed.

V. CONCLUSIONS

In this study, the effects of Ce on the miro- and macrostructure of the as-cast M42 high speed steel were studied. The main conclusions are as follows:

1. The addition of Ce can modify the $MgO{\cdot}Al_2O_3$ and MnS inclusions to the Ce-containing inclusions. When the Ce content is 0.03 wt pct, the inclusions in the steel are Ce_2O_2S. When the Ce contents are 0.16 and 0.27 wt pct, the inclusions in the steels are Ce_2O_2S and Ce_2O_3. The number density and average size of inclusions increases gradually with the increase of Ce content.
2. The addition of Ce is conducive to refining the dendrite structure and eutectic carbides. Both the SDAS and total eutectic carbides content decrease gradually with increasing Ce content. The refining mechanism for the as-cast microstructure is the heterogeneous nucleation of primary austenite (γ-Fe) on Ce_2O_2S or

Table V. Lattice Disregistry Between Eutectic Carbides and Ce_2O_2S or Ce_2O_3

Matching Planes	Matching Directions $[uvw]_s$	Matching Directions $[uvw]_n$	Interatomic Spacing (nm) $d[uvw]_s$	Interatomic Spacing (nm) $d[uvw]_n$	θ (deg)	f (pct)
$(0001)Ce_2O_2S//(0001)M_2C$	$[\bar{1}100]$	$[\bar{1}2\bar{1}0]$	0.701	0.605	0	13.81
	$[\bar{2}110]$	$[\bar{1}100]$	1.215	1.047	0	
	$[\bar{1}010]$	$[\bar{2}110]$	0.701	0.605	0	
$(0001)Ce_2O_3//(0001)M_2C$	$[\bar{1}100]$	$[\bar{1}2\bar{1}0]$	0.682	0.605	0	11.31
	$[\bar{2}110]$	$[\bar{1}100]$	1.181	1.047	0	
	$[\bar{1}010]$	$[\bar{2}110]$	0.682	0.605	0	
$(0001)Ce_2O_2S//(111)M_6C$	$[\bar{1}2\bar{1}0]$	$[\bar{1}10]$	0.810	0.789	0	2.65
	$[\bar{2}110]$	$[\bar{2}11]$	1.403	1.367	0	
	$[\bar{1}010]$	$[\bar{1}10]$	0.810	0.789	0	
$(0001)Ce_2O_3//(111)M_6C$	$[\bar{1}2\bar{1}0]$	$[\bar{1}10]$	0.788	0.789	0	0.13
	$[\bar{2}110]$	$[\bar{2}11]$	1.365	1.367	0	
	$[\bar{1}010]$	$[\bar{1}10]$	0.788	0.789	0	

Ce_2O_3 during solidification and the increase in both the compositional supercooling at the dendrite forefront and the restriction on the dendrites coarsening. The likely matching directions for γ-Fe with Ce_2O_2S or Ce_2O_3 are $(0001)Ce_2O_2S//(100)\gamma$-Fe and $(0001)Ce_2O_3//(100)\gamma$-Fe, respectively.

3. The carbides in the cast ingots with different Ce contents are all composed of M_2C, M_6C and MC carbides, in which M_2C and M_6C carbides are the predominant precipitates. The increase of Ce content makes the morphology of M_2C carbides change from long lamellar or straight-rod morphology into shorter curved-rod or honeycomb morphology because of the overgrowth of eutectic austenite, but it has no significant effect on the morphology of M_6C carbides.
4. Ce_2O_2S and Ce_2O_3 can serve as the very effective heterogeneous nucleation sites for M_6C carbides due to the low lattice disregistry between them, thus improving markedly the macroscopic distribution of M_6C carbides in the cast ingots and promoting the formation of M_6C carbides at the expense of M_2C carbides. The likely matching directions for M_6C with Ce_2O_2S and Ce_2O_3 are $(0001)Ce_2O_2S//(111)M_6C$ and $(0001)Ce_2O_3//(\bar{1}11)M_6C$, respectively.

ACKNOWLEDGMENTS

This research was sponsored by the National Natural Science Foundation of China [Grant Nos. 51774074 and U1960203], Fundamental Research Funds for the Central Universities [Grant Nos. N172512033 and N2025014], Shanxi Municipal Major Science & Technology Project [Grant No. 20181101014] and Talent Project of Revitalizing Liaoning (XLYC1902046).

REFERENCES

1. H.C. Zhu, Z.H. Jiang, H.B. Li, H. Feng, W.C. Jiao, S.C. Zhang, P.B. Wang, and J.H. Zhu: *ISIJ Int*., 2018, vol. 58, pp. 1267–74.
2. X.F. Zhou, W.L. Zhu, H.B. Jiang, F. Fang, Y.Y. Tu, and J.Q. Jiang: *J. Iron. Steel Res. Int*., 2016, vol. 23, pp. 800–07.
3. D. Bombač, M. Terčelj, M. Fazarinc, and G. Kugler: *Mater. Sci. Eng. A*, 2017, vol. 703, pp. 438–50.
4. Y.W. Luo, H.J. Guo, X.L. Sun, J. Guo, and F. Wang: *Metall. Mater. Trans. A*, 2018, vol. 49A, pp. 5976–86.
5. R. Colaço, E. Gordo, E.M. Ruiz-Navas, M. Otasevic, and R. Vilar: *Wear*, 2006, vol. 260, pp. 949–56.
6. Y.W. Luo, H.J. Guo, X.L. Sun, and J. Guo: *Sci. Rep*., 2018, vol. 8, p. 4328.
7. M.A. Hamidzadeh, M. Meratian, and A. Saatchi: *Mater. Sci. Eng. A*, 2013, vol. 571, pp. 193–98.
8. L. Lu, L.G. Hou, J.X. Zhang, H.B. Wang, H. Cui, J.F. Huang, Y.A. Zhang, and J.S. Zhang: *Mater. Charact*., 2016, vol. 117, pp. 1–8.
9. M. Boccalini, A.V.O. Corrêa, and H. Goldenstein: *Mater. Sci. Technol*., 1999, vol. 15, pp. 621–26.
10. E.S. Lee, W.J. Park, J. Jung, and S. Ahn: *Metall. Mater. Trans. A*, 2000, vol. 29A, pp. 1395–1404.
11. F.S. Pan, W.Q. Wang, A.T. Tang, L.Z. Wu, T.T. Liu, and R.J. Cheng: *Prog. Nat. Sci. Mater*., 2011, vol. 21, pp. 180–86.
12. W.C. Jiao, H.B. Li, H. Feng, Z.H. Jiang, J. Dai, H.C. Zhu, S.C. Zhang, M.S. Chu, and W. Wu: *ISIJ Int*., 2019, vol. 60, pp. 564–72.
13. M. Boccalini and H. Goldenstein: *Int. Mater. Rev*., 2001, vol. 46, pp. 92–115.
14. A. Schulz, V. Uhlenwinkel, C. Escher, R. Kohlmann, A. Kulmburg, M.C. Montero, R. Rabitsch, W. Schützenhöfer, D. Stocchi, and D. Viale: *Mater. Sci. Eng. A*, 2008, vol. 477, pp. 69–79.
15. H. Feng, H.B. Li, X.L. Wu, Z.H. Jiang, S. Zhao, T. Zhang, D. Xu, S.C. Zhang, H.C. Zhu, B.B. Zhang, and M.X. Yang: *J. Mater. Sci. Technol*., 2018, vol. 34, pp. 1781–90.
16. G.Q. Zhang, H. Yuan, D.L. Jiao, Z. Li, Y. Zhang, and Z.W. Liu: *Mater. Sci. Eng. A*, 2012, vol. 558, pp. 566–71.
17. H.L. Peng, L. Hu, L.J. Li, L.Y. Zhang, and X.L. Zhang: *J. Alloys Compd*., 2018, vol. 740, pp. 766–73.
18. Y.J. Li, Q.C. Jiang, Y.G. Zhao, Z.M. He, and X.Y. Zhong: *J. Rare Earths*, 2000, vol. 18, pp. 132–35.
19. X.F. Zhou, X.Y. Yin, F. Fang, J.Q. Jiang, and W.L. Zhu: *J. Rare Earths*, 2012, vol. 30, pp. 1075–78.
20. Q.X. Liu, D.P. Lu, L. Lu, Q. Hu, Q.F. Fu, and Z. Zhou: *J. Iron. Steel Res. Int*., 2015, vol. 22, pp. 245–49.
21. H.G. Fu, Q. Xiao, and Y.X. Li: *Mater. Sci. Eng. A*, 2005, vol. 395, pp. 281–87.
22. J. Yang, D.N. Zou, X.M. Li, and Z.Z. Du: *J. Iron. Steel Res. Int*., 2007, vol. 14, pp. 47–59.
23. H.C. Zhu, Z.H. Jiang, H.B. Li, H. Feng, S.C. Zhang, G.H. Liu, J.H. Zhu, P.B. Wang, B.B. Zhang, G.W. Fan, and G.P. Li: *Metall. Mater. Trans. B*, 2017, vol. 48B, pp. 2493–2503.
24. S.C. Zhang, H.B. Li, Z.H. Jiang, B.B. Zhang, Z.X. Li, J.X. Wu, S.P. Fan, H. Feng, and H.C. Zhu: *Mater. Charact*., 2019, vol. 152, pp. 141–50.

25. H. Feng, H.B. Li, W.C. Jiao, Z.H. Jiang, M.H. Cai, H.C. Zhu, and Z.G. Chen: *Metall. Mater. Trans. A*, 2019, vol. 50A, pp. 4987–99.
26. S.C. Zhang, Z.H. Jiang, H.B. Li, B.B. Zhang, S.P. Fan, Z.X. Li, H. Feng, and H.C. Zhu: *Mater. Charact.*, 2018, vol. 137, pp. 244–55.
27. H. Feng, Z.H. Jiang, H.B. Li, P.C. Lu, S.C. Zhang, H.C. Zhu, B.B. Zhang, T. Zhang, D.K. Xu, and Z.G. Chen: *Corros. Sci.*, 2018, vol. 144, pp. 288–300.
28. H. Feng, H.B. Li, Z.H. Jiang, T. Zhang, N. Dong, S.C. Zhang, P.D. Han, S. Zhao, and Z.G. Chen: *Corros. Sci.*, 2019, vol. 158, p. 108081.
29. X. Liu, J.C. Yang, L. Yang, and X.Z. Gao: *J. Iron. Steel Res. Int.*, 2010, vol. 17, pp. 59–64.
30. Y. Huang, G.G. Cheng, S.J. Li, and W.X. Dai: *Steel Res. Int.*, 2018, vol. 89, p. 1800371.
31. J. Lan, J.J. He, W.J. Ding, Q.D. Wang, and Y.P. Zhu: *ISIJ Int.*, 2000, vol. 40, pp. 1275–82.
32. L.J. Wang, Y.Q. Liu, Q. Wang, and K.C. Chou: *ISIJ Int.*, 2015, vol. 55, pp. 970–75.
33. C.Y. Yang, Y.K. Luan, D. Li, and Y.Y. Li: *J. Mater. Sci. Technol.*, 2019, vol. 35, pp. 1298–1308.
34. A. Vahed and D.A.R. Kay: *Metall. Trans. B*, 1976, vol. 7, pp. 375–83.
35. Y.H. Qu, J.D. Xing, X.H. Zhi, J.Y. Peng, and H.G. Fu: *Mater. Lett.*, 2008, vol. 62, pp. 3024–27.
36. B.L. Bramfitt: *Metall. Trans.*, 1970, vol. 5, pp. 1987–95.
37. Y.P. Ji, Y.M. Li, M.X. Zhang, and H.P. Ren: *Metall. Mater. Trans. A*, 2019, vol. 50A, pp. 1787–94.
38. M.M. Song, B. Song, S.H. Zhang, Z.L. Xue, Z.B. Yan, and R.S. Xu: *ISIJ Int.*, 2017, vol. 57, pp. 1261–67.
39. J.S. Park, C. Lee, and J.H. Park: *Metall. Mater. Trans. B*, 2012, vol. 43B, pp. 1550–64.
40. J.B. Gu, J.Y. Li, and R.J. Chang: *Metall. Mater. Trans. A*, 2019, vol. 50A, pp. 518–22.
41. M.G. Qu, Z.H. Wang, H. Li, J.Q. Lv, S.H. Sun, and W.T. Fu: *J. Rare Earths*, 2013, vol. 31, pp. 628–33.
42. F.X. Yin, L. Wang, Z.X. Xiao, J.H. Feng, and L. Zhao: *J. Rare Earths*, 2019, https://doi.org/10.1016/j.jre.2019.09.009.
43. C. Ai, L. Liu, J. Zhang, M. Guo, Z.R. Li, T.W. Huang, J. Zhou, S.S. Li, S.K. Gong, and G. Liu: *J. Alloys Compd.*, 2018, vol. 754, pp. 85–92.
44. G. Li, P. Lan, J.Q. Zhang, and G.X. Wu: *Metall. Mater. Trans. B*, 2020, vol. 51B, pp. 452–66.
45. M. Easton, C. Davidson, and D. St John: *Metall. Mater. Trans. A*, 2010, vol. 41A, pp. 1528–38.
46. T. Sivarupan, C.H. Caceres, and J.A. Taylor: *Metall. Mater. Trans. A*, 2013, vol. 44A, pp. 4071–80.
47. T. Sivarupan, J.A. Taylor, and C.H. Cáceres: *Metall. Mater. Trans. A*, 2015, vol. 46A, pp. 2082–2107.
48. X.F. Zhou, F. Fang, G. Li, and J.Q. Jiang: *ISIJ Int.*, 2010, vol. 50, pp. 1151–57.
49. Y.W. Luo, H.J. Guo, X.L. Sun, J. Guo, and F. Wang: *JOM*, 2020, vol. 72, pp. 326–32.
50. A.S. Chaus: *Met. Sci. Heat Treat.*, 2004, vol. 46, pp. 415–22.
51. J. Hufenbach, A. Helth, M.H. Lee, H. Wendrock, L. Giebeler, C.Y. Choe, K.H. Kim, U. Kühn, T.S. Kim, and J. Eckert: *Mater. Sci. Eng. A*, 2016, vol. 674, pp. 366–74.
52. X.F. Zhou, F. Fang, Y.Y. Tu, J.Q. Jiang, W.L. Zhu, and S.Y. Yin: *J. Southeast Univ.*, 2014, vol. 30, pp. 445–48.
53. J.A. Golczewski and H.F. Fischmeister: *Z. Metallkd.*, 1993, vol. 84, pp. 860–66.